Atmospheric Environment 192 (2018) 35–47

Contents lists available at ScienceDirect

Atmospheric Environment

journal homepage: www.elsevier.com/locate/atmosenv

A long-term source apportionment of $PM_{2.5}$ in New York State during 2005–2016

Stefania Squizzato[a], Mauro Masiol[a], David Q. Rich[a,b], Philip K. Hopke[a,c,*]

[a] Department of Public Health Sciences, University of Rochester School of Medicine and Dentistry, Rochester, NY 14642, USA
[b] Department of Environmental Medicine, University of Rochester School of Medicine and Dentistry, Rochester, NY 14642, USA
[c] Center for Air Resources Engineering and Science, Clarkson University, Potsdam, NY 13699, USA

ARTICLE INFO

Keywords:
Source apportionment
Positive matrix factorization
$PM_{2.5}$
New York state

ABSTRACT

The development and implementation of effective policies for controlling $PM_{2.5}$ mass concentrations and protecting human health depend upon the identification and apportionment of its sources. In this study, the $PM_{2.5}$ sources affecting 6 urban and 2 rural sites across New York State during the period 2005–2016 were determined. The extracted profiles were compared to identify state-wide common profiles. The source contributions provide detailed, long-term quantification of the emission sources across the state during the investigated period (2005–2016). Seven factors were common to all sites: secondary sulfate, secondary nitrate, spark-ignition emissions, diesel emissions, road dust, biomass burning, and pyrolyzed organic (OP) rich. The largest contributors were secondary sulfate, secondary nitrate, spark-ignition (gasoline), diesel, and OP-rich. Secondary sulfate concentrations ranged from 2.3 $\mu g\,m^{-3}$ at Whiteface to 3.2 $\mu g\,m^{-3}$ at Buffalo and the Bronx. The highest secondary sulfate fractional contributions were found at the rural sites (~46% of $PM_{2.5}$ mass) also showed the highest OP-rich contributions (~19%). Secondary nitrate showed the highest concentrations at the urban sites representing ~17% of $PM_{2.5}$ mass (1.6 ± 0.3 $\mu g\,m^{-3}$ on average). Urban sites also showed the highest average spark-ignition concentrations (1.7 ± 0.2 $\mu g\,m^{-3}$, ~18%) and diesel emissions (1.0 ± 0.2 $\mu g\,m^{-3}$, ~10%). During this period, secondary sulfate concentrations declined likely related to the implementation of mitigation strategies for controlling SO_2 emissions and the changing economics of electricity generation. Similarly, diesel and secondary nitrate showed decreases in concentrations likely associated with the introduction of emissions controls and improved quality fuels for heavy-duty diesel on-road trucks and buses. Spark-ignition concentrations showed an increase across the state during 2014–2016 associated with the increase of registered vehicles in New York State.

1. Introduction

Long-term exposure to fine particulate matter (aerodynamic diameter ≤ 2.5 μm; $PM_{2.5}$) has been extensively and consistently associated with many serious adverse human effects, including cardiovascular (Cesaroni et al., 2014; Gardner et al., 2014; Puett et al., 2009), respiratory (Peacock et al., 2011; Weichenthal et al., 2016), neurological (Kioumourtzoglou et al., 2016), cerebrovascular (Santibañez et al., 2013; Stafoggia et al., 2014) diseases, lung cancer (Raaschou-Nielsen et al., 2013; Hamra et al., 2014), and mortality (Krewski et al., 2009; Thurston et al., 2016). Such effects are also detectable for exposures at low ambient concentrations (Shi et al., 2016). Exposure to outdoor air pollution and to particulate matter in outdoor air was included in Group 1 by the International Agency for Research on Cancer, i.e. carcinogenic to human beings (Loomis et al., 2013; Straif et al., 2013).

However, some specific $PM_{2.5}$ characteristics are suspected to be more likely responsible for associations with adverse effects on human health, e.g., mass and number concentrations, chemical composition, size, source, oxidative potential, etc. Since there is still limited knowledge of what specific characteristics may dominate health outcomes (Atkinson et al., 2010; Strak et al., 2012), mass concentration remains the metric adopted for measuring and controlling $PM_{2.5}$ exposure by most jurisdictions, including the United States (U.S.), Canada, China, European Union, and Japan. The development of successful strategies for emission mitigation and the effectiveness of the implementation of measures to abate ambient $PM_{2.5}$ mass concentrations are two major questions addressed by policy makers.

During the past five decades, mitigation strategies have been adopted across the United States to improve air quality at the federal

* Corresponding author. Department of Public Health Sciences, University of Rochester School of Medicine and Dentistry, Rochester, NY 14642, USA.
E-mail address: phopke@clarkson.edu (P.K. Hopke).

https://doi.org/10.1016/j.atmosenv.2018.08.044
Received 10 April 2018; Received in revised form 4 August 2018; Accepted 21 August 2018
Available online 26 August 2018

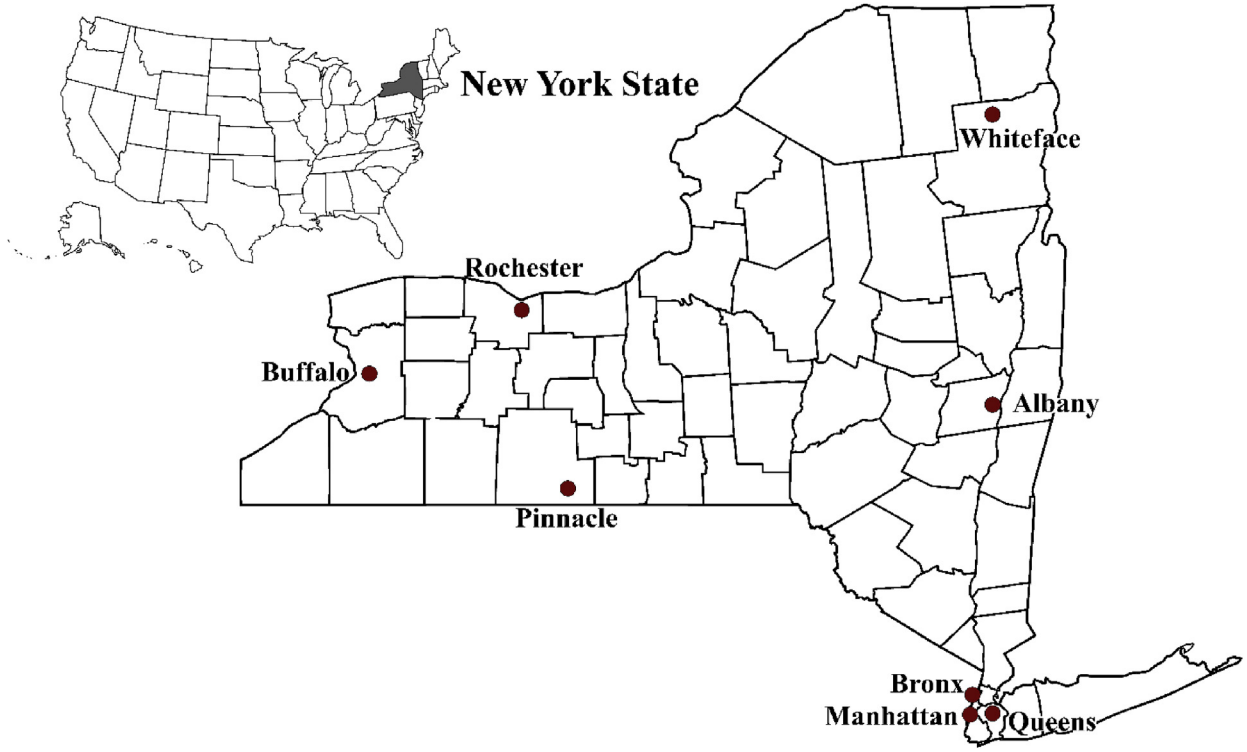

Fig. 1. Monitoring site locations.

and state levels. Since 2000, these strategies were primarily aimed at reducing emissions from light- and heavy-duty vehicles and electric power generation. These strategies include: implementation of Tier 2 standards for light-duty vehicles including computerized engine control and addition of after treatment technologies (2004–2010), the requirement of ultralow sulfur on-road diesel fuel (October 2006), the requirement for particle regenerative traps on new heavy-duty diesel on-road trucks and buses (July 1, 2007), the further requirement for NO_x control for heavy-duty diesel on-road trucks and buses (January 1, 2010), the reduction of sulfur in nonroad diesel fuels between 2010 and 2014, and the NYS requirement that all distillate fuels sold in NYS be ultralow sulfur by July 1, 2012. In New York City, many large buildings were heated by burning No. 6 (residual oil) or No. 4 (mixture of No. 2 and No. 6) oils. Beginning in 2011, permits for using No. 6 oil were disallowed so that by 2015, only No. 4 or cleaner oil could be used. However, No. 4 oil could still contain 1500 ppm S (Kheirbek et al., 2014). New York City claims that between 2011 and 2015, there was a 65% reduction in $PM_{2.5}$ emissions from building heating because of the switch to cleaner fuels (NYC Cleanheat, 2018).

There have also been changes to the upwind sources that emit the precursor gases for particulate sulfate and nitrate including electricity production policy changes in Ontario, Cross-State Air Pollution Rule, and settlement of environmental lawsuits (Emami et al., 2018; Masiol et al., 2018; Squizzato et al., 2018). In addition, there have been substantial changes in electricity generation resulting from the changes in the relative prices of coal and natural gas. Squizzato et al. (2018) reported that decreased electricity production with coal and increased natural gas combustion led to decreases in $PM_{2.5}$ and gaseous pollutants across NYS. They also report that the 2008 economic recession resulted in additional decreases in $PM_{2.5}$ and primary gaseous pollutants concentrations.

The development and implementation of policies for controlling ambient $PM_{2.5}$ mass concentrations and for protecting human health depend upon the analysis of the occurrence, strength, spatial distribution and variability of the sources (Watson et al., 2002; Hopke et al., 2006; Viana et al., 2008). Airborne particles can be emitted from different sources, may be internally and externally mixed and continuously change their composition in space and time due to the complex interplay of atmospheric chemistry, deposition, atmospheric circulation and transport of air masses from regional, continental, and remote regions. However, progress has been made in developing data analysis tools for the detection and quantification of source emissions using compositional data (Hopke, 2015a; b). Receptor models has become very widely used. The most commonly used method is positive matrix factorization (PMF) (Hopke, 2016).

In this study, $PM_{2.5}$ sources across New York State (NYS) were investigated at 8 sites representative of different urban and rural environments over the period of 2005–2016. PMF analysis was applied to chemically-speciated data collected by the NYS Department of Conservation (DEC) as part of the Chemical Speciation Network. The extracted profiles were compared to provide a state-wide dataset of profiles for the common $PM_{2.5}$ sources. The source contributions provide a detailed and long-term quantification of the emission sources across the state.

2. Materials and methods

2.1. Sampling region: New York State

Fann et al. (2012) estimated that Northeast States are affected by the highest $PM_{2.5}$-related premature mortality in the U.S. along with Southeast, and Midwestern geographic regions. The main reasons driving this estimation were attributed to the concurrence of poor air quality ($PM_{2.5}$ and ozone), population density, and baseline health status. Among the northeastern states, NYS represents an interesting case study. It extends over 141×10^3 km^2 and has a total population of $\sim 19.4 \times 10^6$ inhabitants (2010 Census). Although most of the population lives in a few major metropolitan areas (New York City (NYC): 13×10^6 inhabitants in NYS; Buffalo: 1.1×10^6 inhabitants; Rochester: 1.1×10^6 inhabitants; Albany: 0.8×10^6 inhabitants), about 6×10^6 people live in villages and smaller urban areas distributed over a variety of different geomorphological features. NYS is prevailingly hilly, but it

spans from coastal environments and the Allegheny Plateau to the south, mountain areas in the center (Adirondacks and Catskills), the Great Appalachian Valley to the east and the Great Lakes coastlines to the northwest.

2.2. Sampling sites

From 2005 to 2016, sampling for $PM_{2.5}$ chemical speciation was performed at 8 sites (6 urban and 2 rural) across NYS (Fig. 1). The two rural sites (Whiteface base, WHI and Pinnacle State Park, PIN) are in areas not directly influenced by heavily trafficked roads and/or urban and industrial areas and provide an assessment of background pollutant levels and regionally transported air masses. The six urban sites are representative of citywide pollution in the larger metropolitan areas:

- Albany (ALB), along with Schenectady, Troy, and Saratoga Springs, constitutes the third-most populous metropolitan region in the state;
- Buffalo (BUF) is located on the eastern shores of Lake Erie at the head of the Niagara River and still represents the most industrialized area of the state;
- Rochester (ROC) is located on the southern shore of Lake Ontario;
- Three sites are located within the New York City metropolitan area, including Queens College (QUE), located in a high population density section of Queens County, Bronx (BRO) placed on the roof of the Intermediate School 52 (IS 52), in the South Bronx, and Manhattan sites (MAN) (Canal Street and Division Street), located in Lower Manhattan within a high populated density area ($\sim 10.4 \cdot 10^3$ people/km^2). Data from Canal St. are available from January 2005 to March 2007. The site was moved to Division St. beginning March 23, 2007. Considering the proximity of the two Manhattan sampling sites ($\sim$1 km) and both represent similar Manhattan environments, the two datasets were merged.

Detailed descriptions of the sampling site characteristics are provided in the supplementary materials (Section S1).

2.3. Experimental

$PM_{2.5}$ chemically speciated data were retrieved from the EPA Chemical Speciation Network (CSN) (AQS, www.epa.gov/aqs). Samples were collected every third or sixth day (Section S1) and analyzed for elemental carbon (EC) and organic carbon (OC) by thermo-optical analysis, major inorganic ions (Na^+, K^+, NH_4^+, NO_3^-, SO_4^{2-}) by ion chromatography, and elements with atomic number ≥ 11 by energy-dispersive x-ray fluorescence (EDXRF).

Details of the CSN network, sampling methods, analytical protocols, and quality assurance are presented by Solomon et al. (2014).

To compensate for OC blanks, OC blank values were estimated following the approach of Tolocka et al. (2001) and Kim et al. (2005) as the intercept of the regression of OC concentrations against $PM_{2.5}$. Concentrations of ions and elements were blank-corrected using the blank field concentrations provided by CSN. Average annual field blanks were calculated for each site and subtracted from all the samples. Values below the Method Detection Limit (MDL) were replaced with MDL/2.

The CSN network underwent changes in both sampling and analytical protocols during the past decade (Solomon et al., 2014). Between 2007 and 2009, CSN methods for the carbonaceous fraction based on NIOSH4050-like Thermal Optical Transmission (TOT) changed to the IMPROVE protocol and Thermal Optical Reflectance (TOR) to obtain consistency between the IMPROVE and CSN networks. Differences between the two EC/OC methods have been reported (e.g., Chow et al., 2007; Watson et al., 2009; Bae et al., 2009; Malm et al., 2011; Rattigan et al., 2011; Cheng et al., 2011a; b) and will affect the source apportionment results. For this reason, the $PM_{2.5}$ compositional data were split into pre-and post-OC/EC sampling/analysis change data sets. The subsequent source apportionment analyses were conducted separately for each site. A detailed discussion of data preparation and treatment is provided in the supplementary materials (section S2).

2.4. PMF analyses

PMF has been described elsewhere (Paatero and Tapper, 1994; Paatero, 1997; Hopke, 2016). US EPA PMF V5 has two new features: (i) displacement (DISP), a tool for exploring realistic bounds of the rotational ambiguity of the best fit (base run) solution and (ii) constraints, a feature to reduce rotational ambiguity and improve the profiles using a priori information about the nature of the sources (Amato et al., 2009; Amato and Hopke, 2012; Brown et al., 2015). Input datasets were prepared according to the procedure of Polissar et al. (1998). Data below the MDLs were set to MDLs/2, with an uncertainty of 5/6 of the corresponding MDL. Data > MDLs were used with uncertainty values equal to the CSN error with the addition of 1/3 of the MDLs. An uncertainty of 20% was assigned to EC and the EC fractions and to OC and the OC fractions, except for OC1 that was set to 35% to account for adsorption of semivolatiles on the quartz filter fibers. The uncertainty of the total variable ($PM_{2.5}$) was set to 300% and it was then marked as "weak" that multiplied the uncertainties by a factor of 3 to ensure it had no influence on the fits. Only cases reporting $PM_{2.5}$ mass, elements, ions, OC and EC were included into the PMF analysis.

The best solutions were identified according to several criteria and guidelines (Reff et al., 2007; Belis et al., 2014; Brown et al., 2015; Hopke, 2016): (i) knowledge of sources affecting the study area, (ii) the *Q*-value with respect to the expected (theoretical) value and its stability over multiple runs (n = 200), (iii) number of absolute scaled residuals greater than ± 3, and (iv) finding profile uncertainties calculated by bootstrap (BS, n = 200) and displacement (DISP) methods within an acceptable range (Paatero et al., 2014). Further details are provided in the supplementary materials (Section S3).

2.5. Data post-processing

The investigated period was divided into 3 sub-periods (2005–2007, 2008–2013, and 2014–2016) to assess the main changes in $PM_{2.5}$ composition and source contributions relative to known changes in emissions and economic changes including the 2008 recession and the low price of natural gas that has driven changes in electricity generation fuel. These sub-periods represent the pre- (2005–2007), during- (2008–2013) and post- (2014–2016) periods with respect to the implementation of several mitigation strategies. Data were analyzed using R (R Core Team, 2018) and a series of supplementary packages, including 'openair' (Carslaw and Ropkins, 2012; Carslaw, 2018), and 'PMCMR' (Pohlert, 2018). Inter-period differences for the major common $PM_{2.5}$ sources were tested using the non-parametric Kruskal Wallis ANOVA on ranks and the post-hoc Dunn test for the pair-wise comparisons. Temperature and wind data recorded as near to the sites as possible were retrieved from the NCDC - National Climate Data Center (https://www.ncdc.noaa.gov/cdo-web/). Wind data were used as input for computing conditional bivariate probability functions (CBPFs) to assess the PMF results for local source locations. CBPF assesses the probability that source contributions from a given wind direction/speed sector exceed a threshold (75th percentile in this study) by matching wind direction data with source concentrations and by using wind speed as a third variable plotted on the radial axis of bivariate plots. Details of the CBPF analysis are provided by Uria-Tellaetxe and Carslaw (2014).

3. Results and discussion

3.1. $PM_{2.5}$ mass and composition

Temporal variation and trends of $PM_{2.5}$ concentrations and

composition have been already discussed in previous papers (Civerolo et al., 2017; Rattigan et al., 2016; Squizzato et al., 2018). During the investigated period, urban sites had the highest average $PM_{2.5}$concentrations (BRO 11.4 $\mu g\,m^{-3}$, MAN 11.2 $\mu g\,m^{-3}$, QUE 9.5 $\mu g\,m^{-3}$, ALB 8.5 $\mu g\,m^{-3}$, ROC 8.7 $\mu g\,m^{-3}$, BUF 10.1 $\mu g\,m^{-3}$). The lowest average concentrations were observed at the rural sites (PIN 7.6 $\mu g\,m^{-3}$, WHI 5.2 $\mu g\,m^{-3}$). $PM_{2.5}$ was mostly composed of total carbon (TC, expressed as the sum of OC and EC) and secondary inorganic aerosol (SIA, expressed as the sum of NH_4^+, NO_3^-, SO_4^{2-}). Contributions to $PM_{2.5}$ mass ranged between 49% and 39% for SIA and 17%–39% for TC accounting for 68%–78% of the measured mass concentrations.

Common seasonal patterns were detected across the state showing the highest average $PM_{2.5}$ concentrations during summer (Squizzato et al., 2018). Urban sites also showed increased concentration during the cold months (Fig. S1). Similarly, most of the analyzed species exhibited statistically significant seasonal differences (Kruskal-Wallis, p-value < 0.05). The seasonal distributions of the main $PM_{2.5}$ species (SO_4^{2-}, NO_3^-, OC, EC) are presented in supplementary materials (Fig. S1) along with K^+, Na^+ and some selected elements (Figs. S2 to S5).

The combined effects of mitigation strategies and economic drivers resulted in a substantial decrease in $PM_{2.5}$ across the state with slopes calculated using the nonparametric Theil-Sen regression ranging from $-8.6\%\ y^{-1}$ and $-2.2\%\ y^{-1}$, with the largest decrease during summer months (Squizzato et al., 2018). Rattigan et al. (2016) observed a downward trend for most of the major $PM_{2.5}$ species (SO_4^{2-}, NO_3^- and NH_4^+) and selected metals (Se and Ni) in New York State since 2000. Similarly, Emami et al. (2018) reported consistent negative trends for the major $PM_{2.5}$ species measured in Rochester between 2001 and 2016 that were similar to the decline in submicron particle number concentrations (Masiol et al., 2018). Across the state, SIA fractional contributions to $PM_{2.5}$ dropped from 56% (6.8 ± 5.4 $\mu g\,m^{-3}$) on average during 2005–2007 to 36% (2.8 ± 2.4 $\mu g\,m^{-3}$) on average during 2014–2016. The drop is mostly attributable to decreased SO_4^{2-} concentrations that ranged from a mean of 30% (3.6 ± 3.2 $\mu g\,m^{-3}$) during 2005–2007 to −17% (1.2 ± 0.9 $\mu g\,m^{-3}$) during 2014–2016 (Fig. S6). Emami et al. (2018) investigated the upwind SO_2 source impacts in Rochester and reported that the regional sources of sulfate were related to state-level changes in SO_2 emissions from several states.

Despite efforts to reduce NO_x emissions, NO_3^- did not experience as large a decline as SO_4^{2-}. Average NO_3^- concentrations ranged from 1.5 ± 1.6 $\mu g\,m^{-3}$ to 1.1 ± 1.6 $\mu g\,m^{-3}$ during 2005–2007 and 2014–2016, respectively, with similar fractional contributions to $PM_{2.5}$ mass (12% and 13%) (Fig. S7). However, nitrate concentrations are statistically significant different between 2005-2007 and 2014–2016 ($p < 0.005$) at all urban sites expect ALB (Fig. S7) and no statistically significant difference were observed between 2008-2013 and 2014–2016 periods at QUE, BUF, and ALB. Rural sites did not show significant changes among these periods. The lower drop of nitrate concentrations may be associated with the secondary inorganic aerosol formation dynamic. At low NH_3 concentrations, the neutralization of acidic sulfate by ammonia is favored over the formation of ammonium nitrate (Seinfeld and Pandis, 2016). Decreased SO_2 emissions and lower acidic sulfate concentrations resulted in higher availability of ammonia thereby favoring the formation of ammonium nitrate even with decreased NO_x emissions.

The changes in the sampling and analytical methods for OC/EC needed to be addressed in the interpretation of EC and OC in the profiles. The organic carbon concentrations were strongly affected by the changes because OC is more sensitive to filter face velocity, shipment and transport conditions, and analytical methodology (Rattigan et al., 2016). OC_TOT is approximately 50% higher than OC_TOR, whereas the impact on EC is less pronounced with the EC_TOT 5–8% lower than EC_TOR (Rattigan et al., 2016). A significant drop in EC concentrations was observed across the state between the 2008–2013 and 2014–2016 periods. ALB showed statistically significant difference also between 2005-2007 and 2008–2013 (Fig. S8), but $PM_{2.5}$ samples were only collected since August 2007.

Primary and secondary organic carbon (POC and SOC) were estimated by using the EC-tracer method (Cabada et al., 2004). Details are provided in the supplementary materials (Section S4.1, Figs. S9 and S10). POC exhibited a consistent downward trend among the periods at the urban sites except for Albany (Fig. S11). EC and POC trends at rural sites might be more influenced by the monitor and analysis changes because the concentrations are at or near the detection limit as observed by Rattigan et al. (2016). However, while the decreased POC concentrations between 2005-2007 and 2008–2013 can be attributed to the change in EC/OC measurements, the further reduction in EC and POC concentrations during 2014–2016 might be the results of the reduction of primary emissions. Similarly, SOC showed a drop in concentration between 2005-2007 and 2008–2013 likely related to the methodological changes, and a small but significant increase in concentrations during 2014–2016 at ROC, ALB, BRO, MAN, and PIN (Fig. S12). The hypothesis is SO_2 and NO_x reductions permitted more of the atmospheric hydroxyl radicals to react with volatile organic compounds to produce SOC since the reaction rates for hydroxyl with SO_2 and NO_x are substantially faster than with organic species (Seinfeld and Pandis, 2016).

3.2. $PM_{2.5}$ sources

Different numbers of factors were explored before selecting optimal solutions for each data set. The chosen solution had (i) the most physically plausible results; (ii) all runs converged; (iii) stable Q values over 200 runs; and (iv) Q_{true}/Q_{exp} ratio ~1; (v) fewer swaps in bootstrap analysis over 200 runs (BS) and no unmapped factors and (vi) no swaps in displacement analysis (DISP). The obtained PMF models show very good agreement between the predicted and the measured $PM_{2.5}$ mass with high r^2, ranging between 0.89 at PIN and 0.95 at BRO, low intercept, and close to unit slope (~0.9). Detailed PMF results at each site are reported in the supplementary materials (Section S5). At least seven factors were extracted at all sites: (i) secondary sulfate; (ii) secondary nitrate; (iii) spark ignition (gasoline) vehicle emissions; (iv) diesel vehicle emissions; (v) road dust; (vi) biomass burning; (vii) OP-rich. Additionally, road salt was identified as a source in Albany, Buffalo, and Rochester. An aged sea salt source was identified at the Pinnacle, Whiteface, and New York City sites. Fresh sea salt and residual oil were identified only at the New York City sites. An industrial source was extracted for Buffalo. Table 1 reports the identified sources, and the $PM_{2.5}$ contributions for each extracted factor at each site during the pre- and post-OC/EC change periods. Similar source profiles were extracted at all sites within the rotational variability identified by the DISP analyses, i.e. each source has a common profile across the state. The DISP analysis shows the extent of rotational ambiguity in the solution (Paatero et al., 2014). The profiles have relatively small DISP intervals for the dominant species in a given profile and broader ranges for those species for which that source is not an important contributor to it concentration in the samples.

Given the consistency in source profiles between pre- and post-OC/EC changes, the time series of source contributions were merged to yield annual variations (Fig. 2), monthly (Figs. 3–5) and day-of-the-week average patterns (Figs. S45 to S47). Source contribution distributions for the common $PM_{2.5}$ sources during the pre-, during-, and post-periods and the results of Kruskal-Wallis tests are reported in the supplementary materials (Figs. S48 to S58).

3.2.1. Secondary sulfate

Similar secondary sulfate profiles were extracted at all sites characterized by high explained variation and contribution of sulfate and ammonium but also a large share of OC fractions and EC (EC1). High explained variation for Se was generally associated with this factor, supporting the association of secondary sulfate with coal-fired power

Table 1
Average source contributions (in $\mu g\ m^{-3}$ ± standard deviation) on $PM_{2.5}$ mass for each identified sources at each site.

Source	Secondary sulfate	Secondary nitrate	Spark-ignition	Diesel	Road dust	Biomass burning	OP-rich	Aged sea salt	Road salt	Fresh sea salt	Residual oil	Industrial
Albany												
pre-OC/EC change	4.0 ± 5.5	1.6 ± 1.8	1.5 ± 1.5	1.9 ± 1.7	0.4 ± 0.5	0.5 ± 0.5			0.1 ± 0.3			
post-OC/EC change	2.1 ± 2.0	0.9 ± 1.3	2.2 ± 2.0	0.5 ± 0.3	0.2 ± 0.2	0.4 ± 0.5	1.2 ± 1.3		0.1 ± 0.5			
Bronx												
pre-OC/EC change	4.3 ± 4.9	3.1 ± 3.9	1.5 ± 1.6	1.4 ± 1.0	0.3 ± 0.3	0.3 ± 0.5		0.8 ± 0.9		0.4 ± 1.1	1.0 ± 1.0	
post-OC/EC change	2.7 ± 3.5	0.7 ± 1.0	2.0 ± 1.9	0.8 ± 0.5	0.4 ± 0.4	0.1 ± 0.2	1.4 ± 1.8	0.4 ± 0.6		0.1 ± 0.3	1.0 ± 1.1	
Buffalo												
pre-OC/EC change	4.4 ± 5.3	1.7 ± 2.2	1.2 ± 1.4	1.9 ± 1.6	0.2 ± 0.2	1.1 ± 1.1			0.5 ± 1.5			0.3 ± 0.3
post-OC/EC change	2.6 ± 3.3	1.6 ± 2.4	1.5 ± 1.7	0.6 ± 0.4	0.2 ± 0.2	0.6 ± 0.7	0.9 ± 1.0		0.0 ± 0.1			0.2 ± 0.1
Manhattan												
pre-OC/EC change	4.5 ± 5.7	3.9 ± 4.4	1.0 ± 0.9	1.6 ± 1.2	1.0 ± 0.8	0.5 ± 0.7		0.7 ± 0.8		0.4 ± 1.0	0.6 ± 0.7	
post-OC/EC change	2.4 ± 2.7	1.1 ± 1.5	1.9 ± 2.0	1.3 ± 0.7	0.5 ± 0.5	0.3 ± 0.3	1.7 ± 2.3	0.6 ± 0.7		0.1 ± 0.2	0.6 ± 0.8	
Queens												
pre-OC/EC change	4.7 ± 5.1	2.2 ± 2.7	1.5 ± 1.5	1.4 ± 1.1	0.5 ± 0.5	0.6 ± 0.7		0.3 ± 0.4		0.3 ± 0.7	0.4 ± 0.5	
post-OC/EC change	2.2 ± 2.3	1.1 ± 1.7	1.7 ± 1.6	0.7 ± 0.5	0.3 ± 0.3	0.3 ± 0.3	0.9 ± 1.0	0.6 ± 0.7		0.1 ± 0.2	0.4 ± 0.5	
Rochester												
pre-OC/EC change	3.6 ± 4.6	2.6 ± 3.3	1.5 ± 1.4	0.4 ± 0.3	0.2 ± 0.2	0.8 ± 1.1			0.2 ± 0.3			
post-OC/EC change	2.1 ± 2.5	1.5 ± 2.3	1.4 ± 1.6	0.8 ± 0.6	0.1 ± 0.1	0.6 ± 0.5	0.6 ± 0.6		0.1 ± 0.2			
Pinnacle												
pre-OC/EC change	4.4 ± 4.8	0.7 ± 1.0	0.6 ± 0.6	1.5 ± 1.4	0.2 ± 0.2	0.3 ± 0.3		0.3 ± 0.4				
post-OC/EC change	2.0 ± 2.3	0.3 ± 0.4	0.5 ± 0.6	0.9 ± 0.8	0.1 ± 0.1	0.4 ± 0.5	1.2 ± 1.3	0.5 ± 0.6				
Whiteface												
pre-OC/EC change	3.6 ± 4.9	0.7 ± 1.3	0.6 ± 0.6	0.2 ± 0.2	0.3 ± 0.4	0.3 ± 0.4		0.2 ± 0.3				
post-OC/EC change	1.2 ± 1.4	0.2 ± 0.3	0.3 ± 0.3	0.4 ± 0.3	0.4 ± 0.4	0.3 ± 0.4	0.9 ± 1.1	0.2 ± 0.2				

plants. Selenium was previously associated with coal combustion in the northeastern US (Dutkiewicz et al., 2006). This factor also explains ~20% of the variability of V, As, and Br at the New York City sites (BRO, MAN, and QUE). At ALB, BUF and ROC, a fraction of Na and Mg are associated with secondary sulfate sources, suggesting the admixture of aged sea salt.

The average contributions of secondary sulfate to $PM_{2.5}$ ranged from 26% ($3.0\ \mu g\ m^{-3}$) at MAN and 48% ($2.3\ \mu g\ m^{-3}$) at WHI. The highest secondary sulfate concentrations were observed during summer driven by the enhanced photochemistry favoring the formation of ammonium sulfate (Fig. 3). During summer, secondary sulfate contributions ranged from $3.7\ \mu g\ m^{-3}$ at WHI (54% of $PM_{2.5}$ mass) to $5.1\ \mu g\ m^{-3}$ at BUF (48% of $PM_{2.5}$ mass) on average. NYC sites also showed a slight increase during winter with average contributions of $2.3\ \mu g\ m^{-3}$ (19% of $PM_{2.5}$ mass), $2.6\ \mu g\ m^{-3}$ (25% of $PM_{2.5}$ mass) and $3.0\ \mu g\ m^{-3}$ (25% of $PM_{2.5}$ mass) at MAN, QUE, and BRO, respectively. The winter increase of secondary sulfate contributions in New York City can be related to the use of residual oil for space heating as previously reported by Masiol et al. (2017a).

Across the state, secondary sulfate exhibited a consistent decrease over the whole period. Despite this, only ROC, QUE, MAN, and WHI showed statistically significant concentrations between 2005-2007 and 2008–2013, while the differences between 2008-2013 and 2014–2016 are significant at all sites (Fig. S48). These decreases can be related to the decrease of coal used for power generation. In 2008 and 2009, coal used for power generation started to decline and natural gas increased both at the state and national level because of changes in the operating costs driven by the relative costs of these fuels (Squizzato et al., 2018). In New York City (NYS), there have also been changes in the building heating fuels. Kheirbek et al. (2014) has reported that beginning in 2011, NYC regulations required the switch from residual oil (No. 6) to lower sulfur content No. 4 or No. 2 oil by 2015 and that No. 4 oil had to reduce its sulfur content to 1500 ppm. New York State required all No. 2 oil to reduce the sulfur content from 2000 to 15 ppm (ultralow sulfur heating oil) as of July 2012.

3.2.2. Secondary nitrate

The secondary nitrate factor was characterized by the high explained variation for nitrate and high values for ammonium, sulfate, OC, and EC fractions. Large concentrations of OC fractions are seen in the secondary sulfate and secondary nitrate factors. The OC is likely due to the condensation of organic aerosol on the pre-existing ammonium sulfate and ammonium nitrate particles since they represent the majority of the fine particle surface area. Acidic particles may also act to catalyze the reaction of organic vapors enhancing SOA formation on the particle surface and resulting in internally mixed aerosol (e.g., Kuwata et al., 2015; Zhang et al., 2007).

On an annual basis, the highest average contributions of secondary nitrate were at the urban sites ranging between $1.0\ \mu g\ m^{-3}$ (12% of $PM_{2.5}$ mass) and $1.9\ \mu g\ m^{-3}$ (24% of $PM_{2.5}$ mass) at ALB and ROC, respectively. The lowest contributions were estimated at the rural sites showing annual means of $0.4\ \mu g\ m^{-3}$ (9% of $PM_{2.5}$ mass) and $0.5\ \mu g\ m^{-3}$ (7% of $PM_{2.5}$ mass) at WHI and PIN, respectively. Seasonally, common patterns were observed among the sites, with the highest concentrations during colder months (November through March) and the lowest during summer. This pattern is associated with the more favorable environmental conditions for ammonium nitrate formation (lower temperatures and higher relative humidity) and the increase in NO_x emissions due to emissions from space heating. Among the sites, BRO and MAN exhibited slightly different patterns. The trend in secondary nitrate concentrations in spring showed a lower slope. This difference can be related associated with relatively constant traffic emissions and high demand for building heat in these highly urbanized locations. BRO and MAN showed substantial reductions in secondary nitrate between 2005-2007 and 2008–2013 (Fig. S49). New York County showed a drop of registered vehicles during 2008–2011 (Fig.

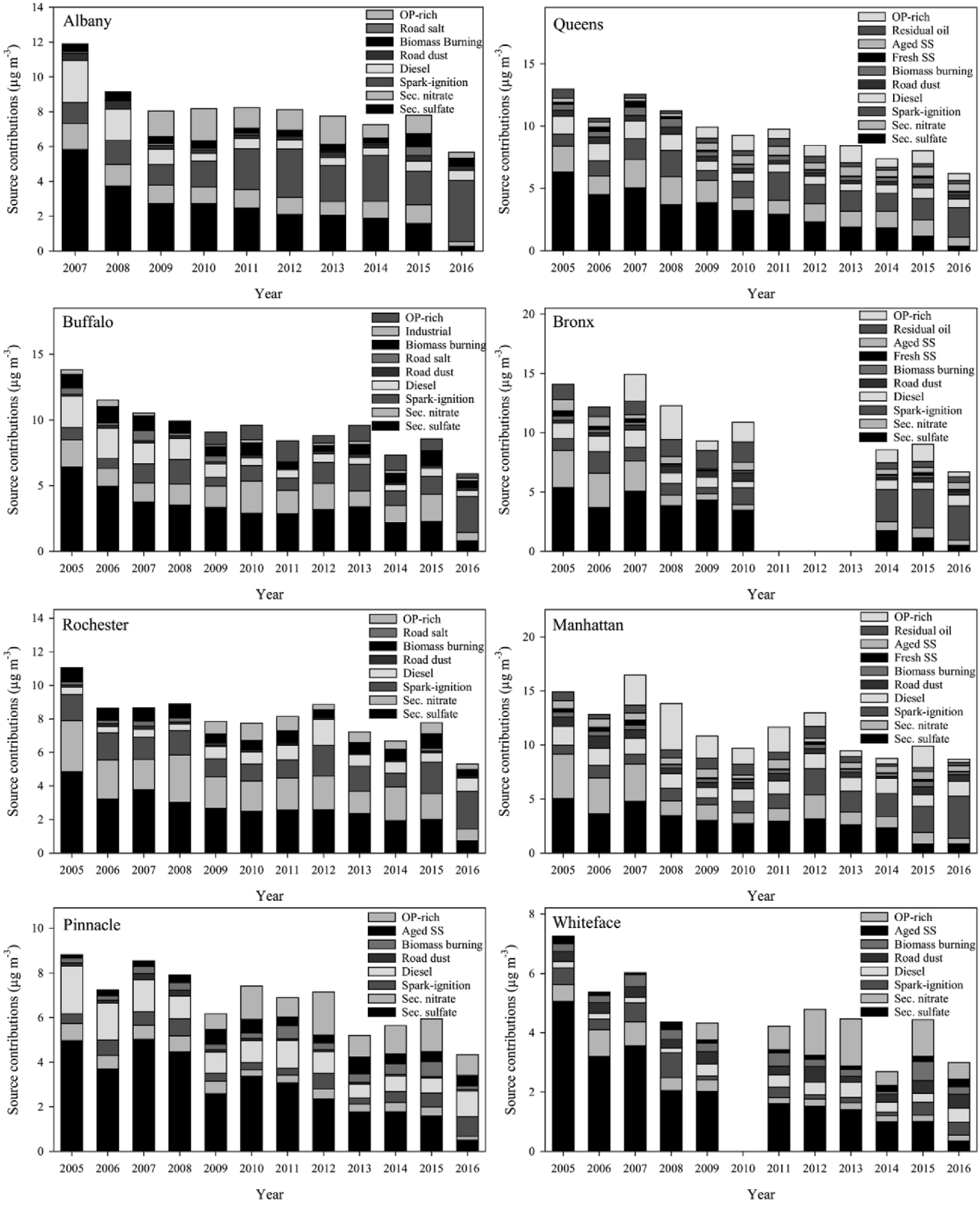

Fig. 2. Annual average estimated source contributions (μg m^{-3}) to $PM_{2.5}$ mass.

S61) that may have caused some of the observed reduction.

3.3. Spark-ignition and diesel vehicle emissions

Temperature-resolved organic and elemental carbon fractions from IMPROVE protocol were frequently used in PMF analysis because enhancing the source separation between spark-ignition (gasoline) and diesel motor exhausts (e.g., Hwang and Hopke, 2007; Kim et al., 2004). However, in this study, NIOSH 4050-like fractions also proved helpful in separating gasoline and diesel emissions in the PMF analyses.

Spark-ignition engines are known to release a higher fraction of OC while diesel engines emit more EC (Pant and Harrison, 2013 and references therein). The spark-ignition emissions factor showed a larger contribution of OC fractions compared to EC, with higher portion of EC1 in the post-OC/EC change PMF. Conversely, diesel factor exhibited higher contributions of EC and explain about 80% of the EC2 variation. Overall, gasoline and diesel profiles were consistent with those observed in previous studies (e.g., Kim et al., 2004; Lee et al., 2006; Zhao

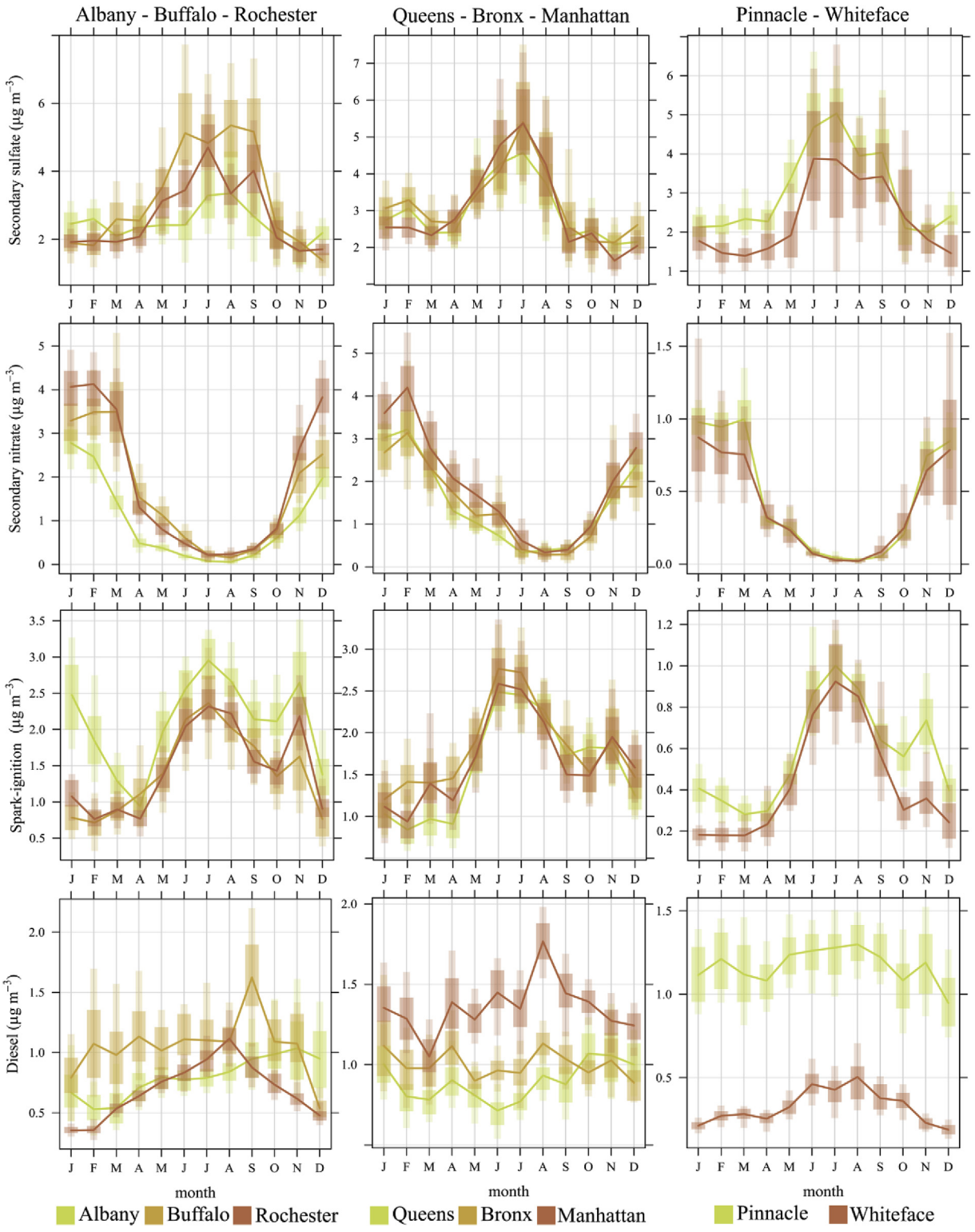

Fig. 3. Seasonal variations of the identified $PM_{2.5}$ sources (secondary sulfate, secondary nitrate, spark-ignition, and diesel). Each plot reports the monthly average and the hourly average concentrations as a filled line and the associated 75th and 99th confidence intervals calculated by bootstrapping the data (n = 200).

and Hopke, 2006).

The elements, Mg, Al, Si, Ca, Fe, Ni, Cu, Zn, and Mn are associated with both gasoline and diesel vehicular traffic factors, but diesel profiles are enriched in Mg, Ca, Ni, Cu, Zn and Mn. Metals can be emitted from various exhaust-related sources including fuel and lubricant combustion, catalytic converters, particulate filters, and engine corrosion. However, these elements more likely arise from non-exhaust sources like brake wear, tire wear, and muffler ablation considering that the amounts of trace elements emitted in the exhaust are very low (Pant and Harrison, 2013 and references therein).

Overall, spark-ignition concentrations were quite similar at the urban sites, ranging from annual means of 1.4–2.1 µg m^{-3} at BUF and ALB, respectively. However, the mean contributions to $PM_{2.5}$ mass varied between 14% and 26% at MAN and ALB, respectively.

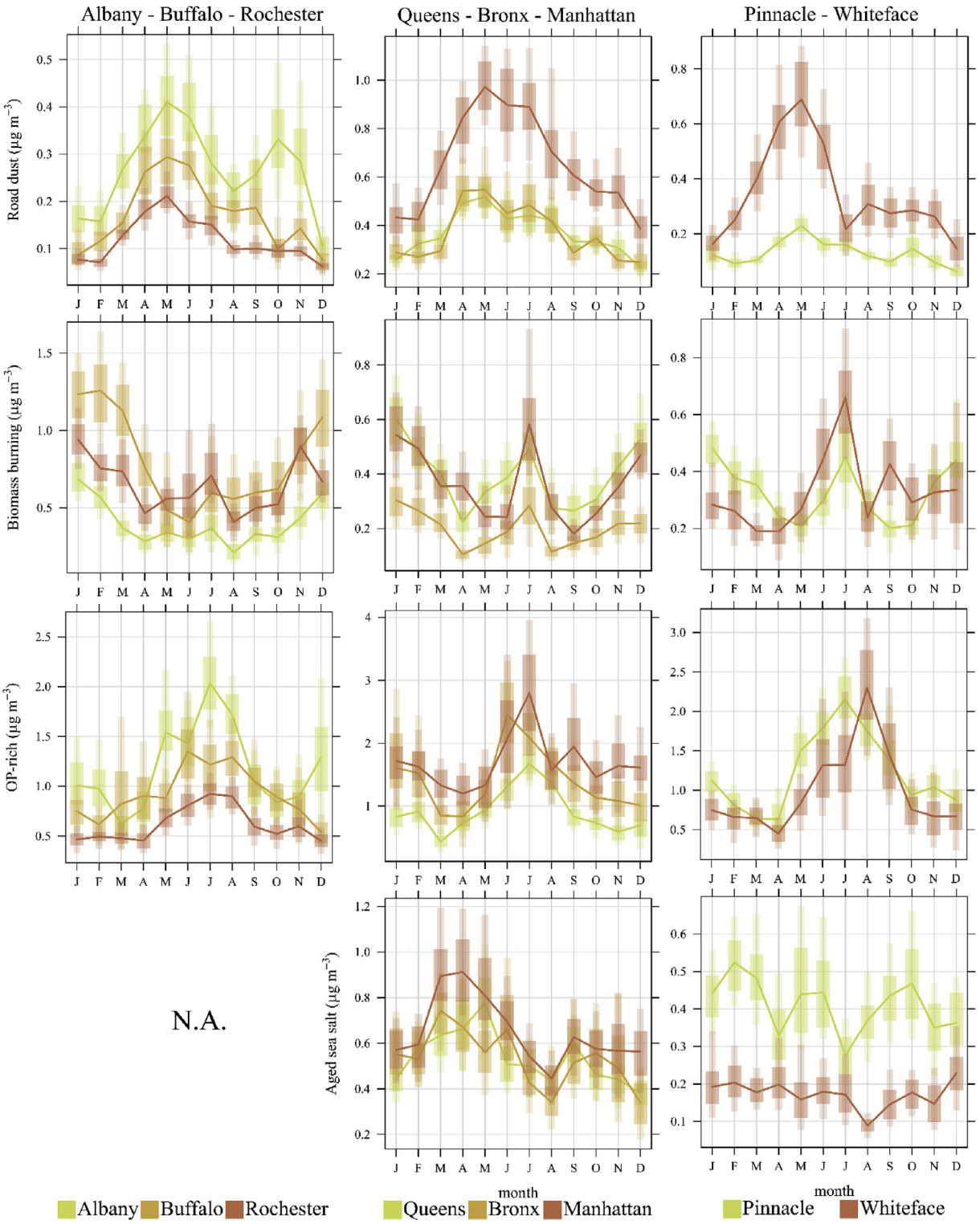

Fig. 4. Seasonal variations of the identified $PM_{2.5}$ sources (road dust, biomass burning, OP-rich, and aged sea salt). Each plot reports the monthly average and the hourly average concentrations as a filled line and the associated 75th and 99th confidence intervals calculated by bootstrapping the data (n = 200).

Seasonally, the spark-ignition factor showed the highest concentrations during summer and autumn at all sites. During the summer months, average spark-ignition concentrations ranged between 2.2 μg m^{-3} (20% of $PM_{2.5}$ mass) and 2.7 μg m^{-3} (31% of $PM_{2.5}$ mass) at BUF and ALB, respectively. Rural sites showed lower average concentrations (0.8 μg m^{-3} and 0.9 μg m^{-3} at WHI and PIN, respectively) and contributions to $PM_{2.5}$ mass (12% and 10% at WHI and PIN, respectively). Higher summer contributions can be associated with higher SOC as well as an increase of vehicular traffic (Fig. S63). Gasoline vehicles have been recognized as large contributors to SOC formation in urban areas (Bahreini et al., 2012; Gordon et al., 2014, 2013; Hayes et al., 2013; Zhao et al., 2016). Similar to SOC, spark-ignition contributions showed an overall increase during the 2014–2016 period (Fig. S50). This increase is consistent with the increase of registered vehicles in New York State (Fig. S61). The observed increase of SOC during the 2014–2016 period may be related to the increase in gasoline emissions.

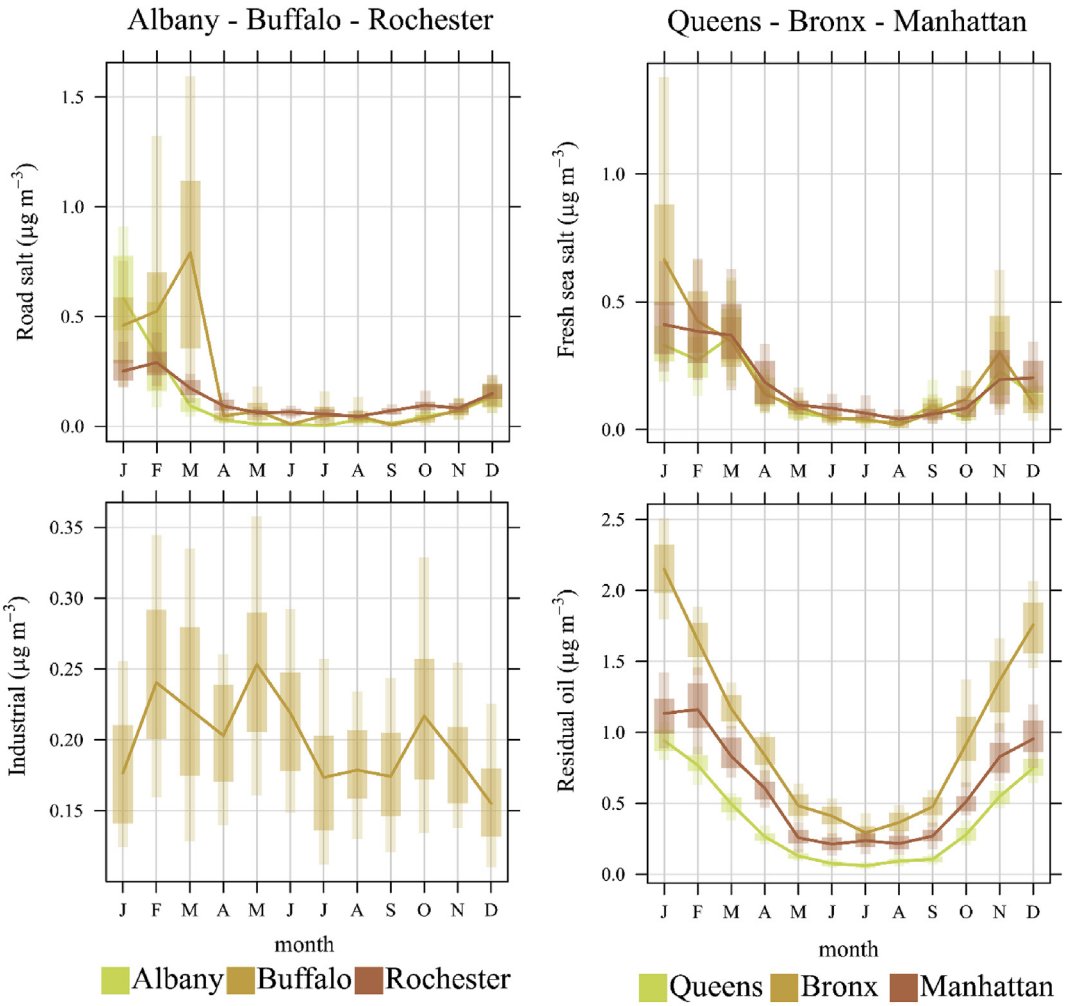

Fig. 5. Seasonal variations of the identified $PM_{2.5}$ sources (road salt, industrial, fresh sea salt, and residual oil). Each plot reports the monthly average and the hourly average concentrations as a filled line and the associated 75th and 99th confidence intervals calculated by bootstrapping the data (n = 200).

On annual average, diesel concentrations ranged from 0.3 µg m^{-3} to 1.4 µg m^{-3} at WHI and MAN, respectively. On a day of week basis, the highest concentrations were observed during working days and the lowest during the weekends at the urban sites (Fig. S45). Percentage contributions to $PM_{2.5}$ mass varied between 7% at WHI and 17% at PIN. The origins of the high diesel contribution to $PM_{2.5}$ at PIN are uncertain. There are no large roads or obvious sources near this site located in a NYS park. However, highest conditional probabilities were associated with winds blowing from south (Fig. S64). This direction pointed to extensive fracking activities in the Marcellus Shale of northern Pennsylvania as the probable source (Fig. S65). Among the shale gas extraction activities, diesel emissions can be related to the use of large diesel-powered equipment during site preparation (e.g., road construction and holding ponds), trucks transporting water, sand, and equipment to the site, and hauling wastewater away, well drilling and hydraulic fracturing, and production of natural gas involving on-site diesel combustion (Litovitz et al., 2013; Moore et al., 2014).

Overall, slightly higher concentrations of diesel emissions were observed during summers (Fig. 3) following the increase of vehicular traffic (Fig. S63). However, a different seasonal pattern can be observed between pre- and post-OC/EC change diesel contributions. This difference can be ascribed to the different seasonal patterns of EC_TOT and EC_TOR (Fig. S66). The change in analytical procedure may have had a significant influence on these patterns.

Across the state, the diesel factor contributions decreased between 2005-2007 and 2008–2013 (Fig. S51) except at ROC and WHI. The largest decreases were observed at ALB and BUF. The ALB sampling site is close the I-787 (~200 m west, and ~400 m north) and the Port of Albany is about 2 km to the south. Buffalo has a similar trend pattern and this sampling site is ~200 m from the I-190. CBPF analysis confirmed these major routes and the Port of Albany as most probable sources of diesel at ALB and BUF (Fig. S65). Lower diesel contributions since 2009 may be due in part to the Clean Heavy-Duty Bus and Truck Rule and cleaner nonroad fuels used by ships docking in Albany. A significant drop in vehicular emissions was observed in the Los Angeles Basin by Hasheminassab et al. (2014a) who reported a significant reduction after 2007 due to the implementation of major federal, state and local regulations.

3.4. Road dust

The road dust factor accounted for high percentages of Al and Si at all sites. Mg, Ca, Fe, Ti, Mn, and Cu exhibited different percentages depending on the sampling location. The source profile also showed relatively large shares of OC fractions, EC (EC fractions), sulfate, nitrate, Na, and Cl. It is well known that road dust represents a mixture of road wear abrasion and particles deposited from other sources (e.g., deicing, biogenic, and geogenic material, exhaust, non-exhaust, demolishing, transport by uncovered trucks, etc.) (Amato et al., 2010; Thorpe and Harrison, 2008). Road surface consists of a mixture of aggregates of various grain size, bitumen, and modifiers such as fillers and adhesives (Thorpe and Harrison, 2008). Al, Si, Ca, Fe, and Mg are

elements usually associated with geological material. However, it is not possible to distinguish between local soil resuspension, road surface abrasion, and local construction activities.

Throughout the period, road dust concentrations varied between 0.1 $\mu g\,m^{-3}$ at PIN and 0.6 $\mu g\,m^{-3}$ at MAN. The highest average fractional contributions to $PM_{2.5}$ mass were at MAN and WHI (6% and 7%, respectively). Seasonally, spring and summer months exhibited the highest average concentrations (Fig. 4) likely due to the combined effects of traffic increase, drier conditions and absence of snow cover.

Road dust exhibited a slight but significant decrease at all sites (Fig. S52) except BRO, showing increased concentrations during 2008–2013. This might be related to construction work activities close to the sampling site.

3.5. Biomass burning

Similar biomass burning source profiles were found at all the sites. This factor was characterized by the highest explained variation for K^+ (50%–88%) and significant shares of OC fractions, EC (mostly EC1), sulfate and nitrate. Other profile components were Na^+ (or Na), Al, Si, Cl, Ca, Fe, Zn and Br. K^+ is widely recognized as marker of biomass burning in source apportionment studies (e.g., Hasheminassab et al., 2014b; Kim et al., 2010; Masiol et al., 2017b; Squizzato et al., 2017). Moreover, biomass burning particles also consist of a mixture of organics, soot, and elements (e.g., Chandrasekaran et al., 2011; Lack et al., 2012; Simoneit, 2002). An increase in ammonium and sulfate was also observed during high biomass burning pollution episodes (Karlsson et al., 2013) explaining higher sulfate than nitrate value in the source profiles. The largest average contributions to $PM_{2.5}$ were observed at ROC and BUF (~8%, 0.6 $\mu g\,m^{-3}$ and 0.8 $\mu g\,m^{-3}$, respectively) followed by BRO and MAN (2% and 3%, respectively), QUE (4%), PIN and ALB (5%), WHI (7%).

Seasonally, the highest average concentrations were reached during winter at all sites ranging from 0.3 $\mu g\,m^{-3}$ to 1.2 $\mu g\,m^{-3}$ at WHI and BUF, respectively (Fig. 4). However, different seasonal patterns can be observed among the sites. ALB, BUF, and ROC exhibited the highest concentrations during colder months and a slight increase during summer. Rural sites and MAN and QUE, showed a more evident increase during summer. High summer concentrations of biomass burning might be ascribed to recreational activities (e.g., barbeques) or long-range transport from wildfires affected areas as previously observed by Masiol et al. (2017b).

The highest biomass burning concentrations were observed during 2005–2007 at the urban sites (Fig. S53). This period was followed by a slight decrease in 2008–2013 and again an increase during 2014–2016. Conversely, PIN and WHI experienced an increase during 2008–2013.

3.6. OP-rich

This factor is only observed when the IMPROVE protocol is used for the OC/EC analyses. It had the highest OP value, and the source profile showed contributions of sulfate (at BRO, MAN, QUE, PIN, and WHI), K^+ (at BRO, BUF, MAN), OC fractions, and EC (EC fractions, at MAN, QUE, PIN, and WHI). The source profiles were consistent with previous studies using OC/EC IMPROVE data (e.g., Zhao and Hopke, 2006; Hwang and Hopke, 2007) where secondary organic aerosol was suggested as the main contributor to this factor. The K^+ is likely related to distant wood/biomass burning since prior work has suggested that large, distant wildfires also contributed to the factor (Kim and Hopke, 2004; Kim et al., 2004). Thus, this factor represents aged secondary aerosol that likely includes more highly oxidized SOC that has condensed and aged in transit along with occasional wildfire plumes that affect NYS.

The co-occurrence of OP and sulfate may represent additional secondary organic aerosol formation caused by the heterogeneous acidic catalyzed reaction between the acidic SO_4^{2-} and gaseous organic compounds (Jang et al., 2003) and the condensation of semi-volatile organic compounds onto acid sulfate particles (Zhao and Hopke, 2006). Fig. S70 presents the scatterplots between OP and the estimated SOC concentrations. At the rural sites, the relationship between OP and SOC is almost linear, supporting the use of OP as a marker of SOA. However, urban sites showed a different relationship. There is a clear edge between OP and SOC at urban sites, but high SOC concentrations occurred in conjunction with low OP concentrations. Thus, the SOC is present from SOA formation and as pyrolytic carbon from biomass burning. Recent work by Robinson and coworkers (Zhao et al., 2016 and references therein) has suggested an increased role for intermediate volatility organic compounds (IVOCs) that are primarily emitted by gasoline vehicles.

Overall, OP-rich contributions ranged on average from 0.6 $\mu g\,m^{-3}$ to 1.7 $\mu g\,m^{-3}$ at ROC and MAN, respectively. Seasonally, the highest concentrations were reached during summer at all sites ranging between 0.9 $\mu g\,m^{-3}$ at ROC and 2.1 $\mu g\,m^{-3}$ at MAN. At the same time, rural sites showed the highest contributions to $PM_{2.5}$ mass. OP-rich contributed on average for 22% and 23% of $PM_{2.5}$ at PIN and WHI, respectively. ALB, BRO, and MAN also showed an increase during winter (Fig. 4). Along the period, OP-rich concentrations exhibited a statistical significant decrease (Fig. S54) except at PIN where no differences were observed.

3.7. Aged sea salt

The aged sea salt factor was characterized by a high explained variation for Na^+ (Na, explained variation > 80%) and Mg. Furthermore, the source profile showed high sulfate and nitrate concentrations, OC fractions and EC (EC fractions) and very low Cl. The lack of Cl is due to the displacement of Cl by strong acidic gases (H_2SO_4 and HNO_3), resulting in the formation of sulfate and nitrate salts. Laskin et al. (2012) indicated there is substantial chemical reactivity between sea salt particles and secondary organic compounds. This factor accounted for ~6% of $PM_{2.5}$ at BRO, MAN, QUE, and PIN and ~4% at WHI with concentrations ranging from 0.2 $\mu g\,m^{-3}$ at WHI and 0.7 $\mu g\,m^{-3}$ at MAN. Seasonally, NYC sites showed a slight increase during spring and autumn whereas rural sites did not exhibit any seasonal pattern (Fig. 4).

At the NYC sites, highest conditional probabilities were associated with strong winds blowing from the east and south-east (Fig. S71). Similarly, Masiol et al. (2017b) reported that southeastern U.S. coastal areas were the probable origin for the aged sea salt observed at QUE. WHI and PIN showed the highest conditional probabilities with southwesterly winds. Aged sea salt was not resolved at BUF, ROC, or ALB. However, the sulfate profiles are enriched in Na suggesting that the aged sea salt factor has been subsumed into the sulfate factor.

3.8. Road salt

The road salt factor explained ~80% of chlorine variation and showed high OC, EC, nitrate, and sulfate, Si, Ca, and Fe. The presence of moderate amounts of Si, Ca and Fe might be linked to the resuspension of crustal particles from the road surface. For colder temperatures, $CaCl_2$ is used to provide greater freezing point depression than can be obtained with NaCl. In recent years, road salt is often mixed with sand to reduce the impact of the saline runoff on ground and surface water while providing adequate traction on slippery roads.

This factor exhibited the highest average concentrations during winter at the urban sites of ALB, BUF, and ROC (0.4 $\mu g\,m^{-3}$, 0.3 $\mu g\,m^{-3}$ and 0.2 $\mu g\,m^{-3}$) (Fig. 5). BUF and ROC also showed an increase during spring (0.3 $\mu g\,m^{-3}$ and 0.1 $\mu g\,m^{-3}$ on average). Spring and winter peaks were likely associated with the use of sodium chloride for deicing. The application of salts and salty brines to roads is common practice during the winter in many urban environments. Road salts can become aerosolized, thereby injecting sodium and chloride particulate

matter into the atmosphere (Kolesar et al., 2018). Fig. S72 reports the monthly average temperatures and snowfall recorded at BUF and ROC. Kolesar et al. (2018) investigated the relationship between Cl, Na, and snowfall across the U.S. Among the NYS sites, Buffalo exhibited the highest positive correlations between Cl, Na, and snowfall. These high correlations were attributed to road salt application and is consistent with the higher average concentrations of road salt during winter observed at BUF compared to ALB and ROC. The CBPF plots show increased probabilities corresponding to heavily trafficked roads under strong wind conditions that enhance particle resuspension (Fig. S73). At ALB, high probabilities are associated with wind blowing from south and south-east where the I-787 is located. At BUF, the highest probabilities are observed for winds blowing from east, south, and south-west in correspondence of the I-190. ROC exhibited the highest probabilities toward the northeast and east, and from south where the I-590 and I-490, respectively, are located.

3.9. Fresh sea salt

This factor showed the highest explained variation for chlorine (85%–92%), and it exhibited high Na^+ (or Na), Ca and Mg. Observed profiles were consistent with the one described in Masiol et al. (2017b) at QUE during the period April 2009–March 2011. It accounted for ~ 2% of $PM_{2.5}$ mass at BRO, MAN, and QUE with an average concentration of 0.2 $\mu g\,m^{-3}$. Although the source profiles were similar to those observed for the road salt factor, the seasonal patterns were very different. Monthly patterns showed an only a small increase during winter (Fig. 5), likely associated with increased wind speeds (3.1 $m\,s^{-1}$, 5.7 $m\,s^{-1}$, 5.3 $m\,s^{-1}$ at MAN, QUE and BRO, respectively) compared to annual average values of 2.6 $m\,s^{-1}$, 5.0 $m\,s^{-1}$, 4.7 $m\,s^{-1}$ at MAN, QUE and BRO, respectively. The higher wind speed enhances the formation of sea spray aerosol. The CBPF analysis supports this hypothesis. The highest probabilities are seen for high wind speeds from the Atlantic Ocean (Fig. S74) at all sites.

3.10. Residual oil

This factor had high explained variation for Ni, Mn, Zn and Ca. The profiles also exhibited high explained variations for V (49% and 23% at BRO, 25% and 17% at MAN, ~19% at QUE during the pre- and post-OC/EC change periods, respectively). These elements were previously associated with the emissions of residual oil combustion (Qin et al., 2006; Masiol et al., 2017b). In addition, this factor showed high shares of OC fractions, EC (EC fractions), sulfate and nitrate. Along the period, residual oil accounted on average for 4% (0.4 $\mu g\,m^{-3}$), 5% (0.6 $\mu g\,m^{-3}$) and 9% (1.0 $\mu g\,m^{-3}$) of $PM_{2.5}$ mass at QUE, MAN and BRO, respectively.

In the NYC-NJ area, residual oil emissions can be ascribed to several sources (e.g., residual oil combustion for space heating, a large oil refinery just south of Elizabeth, NJ, ship emissions from the NY-NJ harbor, and the container port at the Port of Elizabeth, NJ) (Masiol et al., 2017a; b). This factor showed increased contributions during the winter months (Fig. 5) and a negative correlation with the ambient temperature ($-0.5 < r < -0.6$). This result suggests the burning residual oil for space heating was the major source of residual oil combustion emissions. During winter months, average concentrations ranged from 1.9 $\mu g\,m^{-3}$ at BRO to 0.8 $\mu g\,m^{-3}$ at QUE. Moreover, on a weekly base, slightly lower concentrations were observed during the weekends and Monday at BRO and MAN, likely the results of emissions from central heating systems of the large buildings in NYC. Howard et al. (2012) reported that the Manhattan-Bronx area have a very high energy consumption per block area compared to Queens (http://qsel.columbia.edu/nycenergy/). This attribution is consistent with the estimate of Ni concentrations in NYC (NYCAAS, 2018) highlighting Manhattan and the Bronx as high Ni concentrations areas. CBPF plots further support the hypothesis of space heating with No. 4 and No. 6 oil as the major source (Fig. S75). BRO did not show a preferential wind direction because the site is surrounded by large emitting buildings. Conversely, higher probabilities for wind blowing from NE and from W-NW-SSW were observed at MAN and QUE, respectively. The MAN site is in south Manhattan receiving the emissions from main portion of the island. The QUE site is east of Manhattan/Bronx. A sharp decrease in the contributions at all 3 sites were observed (Fig. S58). It appears that the mandated shift to cleaner fuels has resulted in lower building heating emissions as suggested by Kheirbek et al. (2014).

3.11. Industrial

Despite many industries having closed in the recent years, the Buffalo-Niagara area remains one the most industrialized area of the NYS. Major activities include chemical and metal processing, coke production, and metal recycling. A map of the main industrial facilities is provided in the supplementary materials (Fig. S76). At the beginning of the 20th century, many secondary lead smelters operated in the area (USEPA, 2007). EPA monitoring activities showed that there continued to be elevated lead levels at homes near an old industrial site (USEPA, 2015). This exposure is of significant concern to the population living in this neighborhood (WKBW Buffalo, 2016). A map of the former lead smelter locations is provided in Fig. S77.

The identified industrial source profile showed high explained variations and concentrations for Pb, Fe, Mn, Cu, and Zn. This source also explained 31% and 19% of As and Se variation, respectively. This association reflected the multiple industrial facilities of the Buffalo area. As, Zn, Se, and Pb have been associated with coke production (Weitkamp et al., 2005). Pb, Fe, Mn, Cu, and Zn were generally associated with metal/steel industry, ferrous and non-ferrous smelters and power plants emissions (Taiwo et al., 2014 and references therein).

Considering the number of former and current industrial facilities in the Buffalo area, this factor represents a mixed source of industrial emissions and resuspension from various locations including the former secondary lead smelters located close to the monitoring site. The 2005–2007 period showed the highest industrial contributions (0.3 $\mu g\,m^{-3}$ on average) followed by a minimum during 2008–2009 (0.1 $\mu g\,m^{-3}$ on average) during the 2008 economic recession and a relatively constant contribution from 2010 to 2016 (0.2 $\mu g\,m^{-3}$ on average) (Fig. S24). The CBPF plot showed the highest probabilities for winds blowing from south-west where a large steel processing plant was operating until April 2009 (Fig. S79). The effect of the plant closure is evident in the CBPF plots computed by period (Fig. S80). A source of industrial emissions is likely located southwest of the site during 2005–2007, but it was no longer identifiable during 2008–2013 and 2014–2016 periods.

4. Conclusions

$PM_{2.5}$ sources across the New York State (NYS) were identified at 8 sites representative of different urban and rural environments during the period of 2005–2016. Seven common factors were extracted at all sites: (i) secondary sulfate; (ii) secondary nitrate; (iii) spark-ignition emissions; (iv) diesel emissions; (v) road dust; (vi) biomass burning; (vii) OP-rich. Additionally, a road salt source was identified at Albany, Buffalo, and Rochester. An aged sea salt source was identified at Pinnacle, Whiteface, and New York City sites. Fresh sea salt and residual oil sources were identified only at the New York City sites. Industrial sources were found at Buffalo. Overall, similar source profiles were identified providing a statewide source profile characterization.

The largest contributor to $PM_{2.5}$ mass was represented by secondary sulfate, followed by secondary nitrate, spark-ignition, diesel, and OP-rich. The highest fractional secondary sulfate contributions were reached at the rural sites (~46% of $PM_{2.5}$ mass) also showing the highest OP-rich fractional contributions (~19%). Secondary sulfate concentrations ranged from 2.3 $\mu g\,m^{-3}$ at Whiteface to 3.2 $\mu g\,m^{-3}$ at

Buffalo and Bronx. Secondary nitrate showed the highest concentrations at the urban sites representing on average ~17% of $PM_{2.5}$ mass ($1.6 \pm 0.3\,\mu g\,m^{-3}$). Urban sites also showed the highest average concentrations of spark-ignition ($1.7 \pm 0.2\,\mu g\,m^{-3}$, ~18%) and diesel vehicular emissions ($1.0 \pm 0.2\,\mu g\,m^{-3}$, ~10%).

During this period, secondary sulfate experienced the largest decrease in concentrations likely related to the implementation of mitigation strategies for controlling SO_2 emissions and economic factors such as the 2008 recession and the sharp drop in the price of natural gas. Diesel and secondary nitrate also exhibited decreased concentrations. Spark-ignition vehicle contributions increased across the state during 2014–2016 associated with an increase of the secondary organic carbon (SOC). The spark-ignition increase was consistent with the observed increase of registered vehicles in New York State and may also have been influenced by the decreases in SO_2 and NO_x that resulted in more oxidants being available to react with organic precursors of SOC. These source apportionments will be used in epidemiological studies that are currently in progress. Detailed trends analyses are also being done. They will provide the information needed to assess changes in air quality with respect to these major sources and provide information that will permit better air quality management planning for the near-term future.

Acknowledgments

This work was supported by the New York State Energy Research and Development Authority under agreements #59800, 59802, and 100412.

Appendix A. Supplementary data

Supplementary material related to this article can be found at https://doi.org/10.1016/j.atmosenv.2018.08.044.

References

Amato, F., Hopke, P.K., 2012. Source apportionment of the ambient PM2.5 across St. Louis using constrained positive matrix factorization. Atmos. Environ. 46, 329–337.
Amato, F., Pandolfi, M., Escrig, A., Querol, X., Alastuey, A., Pey, J., Perez, N., Hopke, P.K., 2009. Quantifying road dust resuspension in urban environment by multilinear engine: a comparison with PMF2. Atmos. Environ. 43, 2770–2780.
Amato, F., Moreno, T., Pandolfi, M., Querol, X., Alastuey, A., Delgado, A., Pedrero, M., Cots, N., 2010. Concentrations, sources and geochemistry of airborne particulate matter at a major European airport. J. Environ. Monit. 12, 854–862.
Atkinson, R.W., Fuller, G.W., Anderson, H.R., Harrison, R.M., Armstrong, B., 2010. Urban ambient particle metrics and health: a time-series analysis. Epidemiology 21, 501–511.
Bae, M.S., Schauer, J.J., Turner, J.R., Hopke, P.K., 2009. Seasonal variations of elemental carbon in urban aerosols as measured by two common thermal-optical carbon methods. Sci. Total Environ. 407, 5176–5183.
Bahreini, R., Middlebrook, A.M., De Gouw, J.A., Warneke, C., Trainer, M., Brock, C.A., Stark, H., Brown, S.S., Dube, W.P., Gilman, J.B., Hall, K., Holloway, J.S., Kuster, W.C., Perring, A.E., Prevot, A.S.H., Schwarz, J.P., Spackman, J.R., Szidat, S., Wagner, N.L., Weber, R.J., Zotter, P., Parrish, D.D., 2012. Gasoline emissions dominate over diesel in formation of secondary organic aerosol mass. Geophys. Res. Lett. 39, 2–7.
Belis, C.A., Larsen, B.R., Amato, F., El Haddad, I., Favez, O., Harrison, R.M., Hopke, P.K., Nava, S., Paatero, P., Prévôt, A., Quass, U., Vecchi, R., Viana, M., 2014. European Guide on Air Pollution Source Apportionment with Receptor Models. JRC Reference Reports EUR26080 EN.
Brown, S.G., Eberly, S., Paatero, P., Norris, G.A., 2015. Methods for estimating uncertainty in PMF solutions: examples with ambient air and water quality data and guidance on reporting PMF results. Sci. Total Environ. 518, 626–635.
Buffalo, W.K.B.W., 2016. Lead prompts warning about kids playing outside. Available at: https://www.wkbw.com/news/epa-finds-elevated-lead-levels-at-homes-near-old-industrial-site.
Cabada, J.C., Pandis, S.N., Subramanian, R., Robinson, A.L., Polidori, A., Turpin, B., 2004. Estimating the secondary organic aerosol contribution to PM2.5 using the EC tracer method special issue of aerosol science and technology on findings from the fine particulate matter supersites program. Aerosol Sci. Technol. 38, 140–155.
Carslaw, D.C., 2018. Package "openair". Tools for the Analysis of Air Pollution Data. Available from. http://davidcarslaw.github.io/openair/, Accessed date: February 2018.
Carslaw, D.C., Ropkins, K., 2012. Openair - an r package for air quality data analysis. Environ. Model. Software 27–28, 52–61.
Cesaroni, G., Forastiere, F., Stafoggia, M., Andersen, Z.J., Badaloni, C., Beelen, R., Caracciolo, B., de Faire, U., Erbel, R., Eriksen, K.T., Fratiglioni, L., 2014. Long term exposure to ambient air pollution and incidence of acute coronary events: prospective cohort study and meta-analysis in 11 European cohorts from the ESCAPE Project. BMJ 348, f7412.
Chandrasekaran, S.R., Laing, J.R., Holsen, T.M., Raja, S., Hopke, P.K., 2011. Emission characterization and efficiency measurements of high-efficiency wood boilers. Energy Fuels 25, 5015–5021.
Cheng, Y., He, K.B., Duan, F.K., Zheng, M., Du, Z.Y., Ma, Y.L., Tan, J.H., 2011a. Ambient organic carbon to elemental carbon ratios: influences of the measurement methods and implications. Atmos. Environ. 45, 2060–2066.
Cheng, Y., Zheng, M., He, K.B., Chen, Y., Yan, B., Russell, A.G., Shi, W., Jiao, Z., Sheng, G., Fu, J., Edgerton, E.S., 2011b. Comparison of two thermal-optical methods for the determination of organic carbon and elemental carbon: results from the southeastern United States. Atmos. Environ. 45, 1913–1918.
Chow, J.C., Watson, J.G., Chen, L.W.A., Chang, M.O., Robinson, N.F., Trimble, D., Kohl, S., 2007. The IMPROVE_A temperature protocol for thermal/optical carbon analysis: maintaining consistency with a long-term database. J. Air Waste Manag. Assoc. 57, 1014–1023.
Civerolo, K.L., Rattigan, O.V., Felton, H.D., Schwab, J.J., 2017. Changes in gas-phase air pollutants across New York state, USA. Aerosol Air Qual. Res. 17, 147–166.
Dutkiewicz, V.A., Qureshi, S., Husain, L., Schwab, J.J., Demerjian, K.L., 2006. Elemental composition of PM2.5 aerosols in Queens, New York: evaluation of sources of fine-particle mass. Atmos. Environ. 40, 347–359.
Emami, F., Masiol, M., Hopke, P.K., 2018. Air pollution at Rochester, NY: long-term trends and multivariate analysis of upwind SO2 source impacts. Sci. Total Environ. 612, 1506–1515.
Fann, N., Lamson, A.D., Anenberg, S.C., Wesson, K., Risley, D., Hubbell, B.J., 2012. Estimating the national public health burden associated with exposure to ambient PM2.5 and ozone. Risk Anal. 32, 81–95.
Gardner, B., Ling, F., Hopke, P.K., Frampton, M.W., Utell, M.J., Zareba, W., et al., 2014. Ambient fine particulate air pollution triggers ST-elevation myocardial infarction, but not non-ST elevation myocardial infarction: a case-crossover study. Part Fib Toxicol. 11, 1.
Gordon, T.D., Tkacik, D.S., Presto, A.A., Zhang, M., Jathar, S.H., Nguyen, N.T., Massetti, J., Truong, T., Cicero-Fernandez, P., Maddox, C., Rieger, P., Chattopadhyay, S., Maldonado, H., Maricq, M.M., Robinson, A.L., 2013. Primary gas- and particle-phase emissions and secondary organic aerosol production from gasoline and diesel off-road engines. Environ. Sci. Technol. 47, 14137–14146.
Gordon, T.D., Presto, A.A., May, A.A., Nguyen, N.T., Lipsky, E.M., Donahue, N.M., Gutierrez, A., Zhang, M., Maddox, C., Rieger, P., Chattopadhyay, S., Maldonado, H., Maricq, M.M., Robinson, A.L., 2014. Secondary organic aerosol formation exceeds primary particulate matter emissions for light-duty gasoline vehicles. Atmos. Chem. Phys. 14, 4661–4678.
Hamra, G.B., Guha, N., Cohen, A., Laden, F., Raaschou-Nielsen, O., Samet, J.M., Vineis, P., Forastiere, F., Saldiva, P., Yorifuji, T., Loomis, D., 2014. Outdoor particulate matter exposure and lung cancer: a systematic review and meta-analysis. Environ. Health Perspect. 122, 906–911.
Hasheminassab, S., Daher, N., Ostro, B.D., Sioutas, C., 2014a. Long-term source apportionment of ambient fine particulate matter (PM2.5) in the Los Angeles Basin: a focus on emissions reduction from vehicular sources. Environ. Pollut. 193, 54–64.
Hasheminassab, S., Daher, N., Saffari, A., Wang, D., Ostro, B.D., Sioutas, C., 2014b. Spatial and temporal variability of sources of ambient fine particulate matter (PM2.5) in California. Atmos. Chem. Phys. 14, 12085–12097.
Hayes, P.L., Ortega, A.M., Cubison, M.J., Froyd, K.D., Zhao, Y., Cliff, S.S., Hu, W.W., Toohey, D.W., Flynn, J.H., Lefer, B.L., Grossberg, N., Alvarez, S., Rappenglück, B., Taylor, J.W., Allan, J.D., Holloway, J.S., Gilman, J.B., Kuster, W.C., De Gouw, J.A., Massoli, P., Zhang, X., Liu, J., Weber, R.J., Corrigan, A.L., Russell, L.M., Isaacman, G., Worton, D.R., Kreisberg, N.M., Goldstein, A.H., Thalman, R., Waxman, E.M., Volkamer, R., Lin, Y.H., Surratt, J.D., Kleindienst, T.E., Offenberg, J.H., Dusanter, S., Griffith, S., Stevens, P.S., Brioude, J., Angevine, W.M., Jimenez, J.L., 2013. Organic aerosol composition and sources in Pasadena, California, during the 2010 CalNex campaign. J. Geophys. Res. Atmos. 118, 9233–9257.
Hopke, P.K., 2015a. Chemometrics applied to environmental systems. Chemometr. Intell. Lab. Syst. 149, 205–214.
Hopke, P.K., 2015b. Applying multivariate curve resolution to source apportionment of the atmospheric aerosol in 40 years of chemometrics—from Bruce Kowalski to the Future. In: ACS Symposium Series. American Chemical Society, Washington, DC, pp. 129–157.
Hopke, P.K., 2016. Review of receptor modeling methods for source apportionment. J. Air Waste Manag. Assoc. 66, 237–259.
Hopke, P.K., Ito, K., Mar, T., Christensen, W.F., Eatough, D.J., Henry, R.C., Kim, E., Laden, F., Lall, R., Larson, T.V., Liu, H., Neas, L., Pinto, J., Stö lzel, M., Suh, H., Paatero, P., Thurston, G.D., 2006. PM source apportionment and health effects: 1. Intercomparison of source apportionment results. J. Expo. Sci. Environ. Epidemiol. 16, 275–286.
Howard, B., Parshall, L., Thompson, J., Hammer, S., Dickinson, J., Modi, V., 2012. Spatial distribution of urban building energy consumption by end use. Energy Build. 45, 141–151.
Hwang, I.J., Hopke, P.K., 2007. Estimation of source apportionment and potential source locations of PM2.5at a west coastal IMPROVE site. Atmos. Environ. 41, 506–518.
Jang, M., Lee, S., Kamens, R.M., 2003. Organic aerosol growth by acid-catalyzed heterogeneous reactions of octanal in a flow reactor. Atmos. Environ. 37, 2125–2138.
Karlsson, P.E., Ferm, M., Tømmervik, H., Hole, L.R., Pihl Karlsson, G., Ruoho-Airola, T., Aas, W., Hellsten, S., Akselsson, C., Mikkelsen, T.N., Nihlgård, B., 2013. Biomass burning in eastern Europe during spring 2006 caused high deposition of ammonium in northern Fennoscandia. Environ. Pollut. 176, 71–79.
Kheirbek, I., Haney, J., Douglas, S., Ito, K., Caputo Jr., S., Matte, T., 2014. The public health benefits of reducing fine particulate matter through conversion to cleaner heating fuels in New York city. Environ. Sci. Technol. 48, 13573–13582.
Kim, E., Hopke, P.K., 2004. Improving source identification of fine particles in a rural northeastern U.S. area utilizing temperature-resolved carbon fractions. J. Geophys. Res. Atmos. 109, D09204.

Kim, E., Hopke, P.K., Edgerton, E.S., 2004. Improving source identification of Atlanta aerosol using temperature resolved carbon fractions in positive matrix factorization. Atmos. Environ. 38, 3349–3362.
Kim, E., Hopke, P.K., Qin, Y., 2005. Estimation of organic carbon blank values and error structures of the speciation trends network data for source apportionment. J. Air Waste Manag. Assoc. 55, 1190–1199.
Kim, E., Turkiewicz, K., Zulawnick, S.A., Magliano, K.L., 2010. Sources of fine particles in the South Coast area, California. Atmos. Environ. 44, 3095–3100.
Kioumourtzoglou, M.A., Schwartz, J.D., Weisskopf, M.G., Melly, S.J., Wang, Y., Dominici, F., Zanobetti, A., 2016. Long-term PM2.5 exposure and neurological hospital admissions in the Northeastern United States. Environ. Health Perspect. 124, 23–29.
Kolesar, K.R., Mattson, C.N., Peterson, P.K., May, N.W., Prendergast, R.K., Pratt, K.A., 2018. Increases in wintertime PM2.5 sodium and chloride linked to snowfall and road salt application. Atmos. Environ. 177, 195–202.
Krewski, D., Jerrett, M., Burnett, R.T., Ma, R., Hughes, E., Shi, Y., Turner, M.C., Pope III, C.A., Thurston, G., Calle, E.E., Thun, M.J., 2009. Extended follow-up and spatial analysis of the American Cancer Society study linking particulate air pollution and mortality. Res. Rep. Health Eff. Inst. 140, 5–114.
Kuwata, M., Liu, Y., McKinney, K., Martin, S.T., 2015. Physical state and acidity of inorganic sulfate can regulate the production of secondary organic material from isoprene photooxidation products. Phys. Chem. Chem. Phys. 17, 5670–5678.
Lack, D.A., Langridge, J.M., Bahreini, R., Cappa, C.D., Middlebrook, A.M., Schwarz, J.P., 2012. Brown carbon and internal mixing in biomass burning particles. Proc. Natl. Acad. Sci. Unit. States Am. 109, 14802–14807.
Laskin, A., Moffet, R.C., Gilles, M.K., Fast, J.D., Zaveri, R.A., Wang, B., Nigge, P., Shutthanandan, J., 2012. Tropospheric chemistry of internally mixed sea salt and organic particles: surprising reactivity of NaCl with weak organic acids. J. Geophys. Res. Atmos. 117, 1–12.
Lee, J.H., Hopke, P.K., Turner, J.R., 2006. Source identification of airborne PM2.5 at the St. Louis-Midwest supersite. J. Geophys. Res. Atmos. 111, 1–12.
Litovitz, A., Curtright, A., Abramzon, A., Burger, N., Samaras, C., 2013. Estimation of regional air-quality damages from Marcellus Shale natural gas extraction in Pennsylvania. Environ. Res. Lett. 8 014017.
Loomis, D., Grosse, Y., Lauby-Secretan, B., Ghissassi, F.E., Bouvard, V., Benbrahim-Tallaa, L., et al., 2013. The carcinogenicity of outdoor air pollution. Lancet Oncol. 14, 1262–1263.
Malm, W.C., Schichtel, B.A., Pitchford, M.L., 2011. Uncertainties in PM2. 5 gravimetric and speciation measurements and what we can learn from them. J. Air Waste Manag. Assoc. 61, 1131–1149.
Masiol, M., Hopke, P.K., Felton, H.D., Frank, B.P., Rattigan, O.V., Wurth, M.J., LaDuke, G.H., 2017a. Analysis of major air pollutants and submicron particles in New York City and Long Island. Atmos. Environ. 148, 0–15.
Masiol, M., Hopke, P.K., Felton, H.D., Frank, B.P., Rattigan, O.V., Wurth, M.J., LaDuke, G.H., 2017b. Source apportionment of PM2.5 chemically speciated mass and particle number concentrations in New York City. Atmos. Environ. 148, 215–229.
Masiol, M., Squizzato, S., Rich, D.Q., Hopke, P.K., 2018. Long-term trends in submicron particle concentrations in a metropolitan area of the northeastern United States. Sci. Total Environ. 633, 59–70.
Moore, C.W., Zielinska, B., Pétron, G., Jackson, R.B., 2014. Air impacts of increased natural gas acquisition, processing, and use: a critical review. Environ. Sci. Technol. 48, 8349–8359.
NYC Cleanheat, 2018. https://www.nyccleanheat.org/.
NYCAAS, 2018. Nickel Concentrations in Ambient Fine Particles: Winter Monitoring, 2008-2009. New York City Community Air Survey (NYCCAS). Available at: https://www1.nyc.gov/assets/doh/downloads/pdf/eode/nyccas-nireport0510.pdf, Accessed date: March 2018.
Paatero, P., 1997. Least squares formulation of robust non-negative factor analysis. Chemom. Intell. Lab. 37, 23–35.
Paatero, P., Tapper, U., 1994. Positive matrix factorization: a non-negative factor model with optimal utilization of error estimates of data values. Environmetrics 5, 111–126.
Paatero, P., Eberly, S., Brown, S.G., Norris, G.A., 2014. Methods for estimating uncertainty in factor analytic solutions. Atmos. Meas. Tech. 7, 781–797.
Pant, P., Harrison, R.M., 2013. Estimation of the contribution of road traffic emissions to particulate matter concentrations from fi eld measurements: a review. Atmos. Environ. 77, 78–97.
Peacock, J.L., Anderson, H.R., Bremner, S.A., Marston, L., Seemungal, T.A., Strachan, D.P., Wedzicha, J.A., 2011. Outdoor air pollution and respiratory health in patients with COPD. Thorax 66, 591–596.
Pohlert, T., 2018. PMCMR: calculate pairwise multiple comparisons of mean rank sums. R package version 4.2. http://CRAN.R-project.org/package=PMCMR.
Polissar, A.V., Hopke, P.K., Paatero, P., Malm, W.C., Sisler, J.F., 1998. Atmospheric aerosol over Alaska 2. Elemental composition and sources. J. Geophys. Res. 103, 19045–19057.
Puett, R.C., Hart, J.E., Yanosky, J.D., Paciorek, C., Schwartz, J., Suh, H., Speizer, F.E., Laden, F., 2009. Chronic fine and coarse particulate exposure, mortality, and coronary heart disease in the Nurses' Health Study. Environ. Health Perspect. 117, 1697.
Qin, Y., Kim, E., Hopke, P.K., 2006. The concentrations and sources of PM2.5 in metropolitan New York City. Atmos. Environ. 40, 312–332.
R Core Team, 2018. R: a Language and Environment for Statistical Computing. R Foundation for Statistical Computing, Vienna, Austria. https://www.R-project.org/.
Raaschou-Nielsen, O., Andersen, Z.J., Beelen, R., Samoli, E., Stafoggia, M., Weinmayr, G., Hoffmann, B., Fischer, P., Nieuwenhuijsen, M.J., Brunekreef, B., Xun, W.W., 2013. Air pollution and lung cancer incidence in 17 European cohorts: prospective analyses from the European study of cohorts for air pollution effects (ESCAPE). Lancet Oncol. 14, 813–822.
Rattigan, O.V., Felton, H.D., Bae, M.S., Schwab, J.J., Demerjian, K.L., 2011. Comparison of long-term PM 2.5 carbon measurements at an urban and rural location in New York. Atmos. Environ. 45, 3228–3236.
Rattigan, O.V., Civerolo, K.L., Dirk Felton, H., Schwab, J.J., Demerjian, K.L., 2016. Long term trends in New York: PM2.5 mass and particle components. Aerosol Air Qual. Res. 16, 1191–1205.
Reff, A., Eberly, S.I., Bhave, P.V., 2007. Receptor modeling of ambient particulate matter data using positive matrix factorization: review of existing methods. J. Air Waste Manag. Assoc. 57, 146–154.
Santibañez, D.A., Ibarra, S., Matus, P., Seguel, R., 2013. A five-year study of particulate matter (PM2. 5) and cerebrovascular diseases. Environ. Pollut. 181, 1–6.
Seinfeld, J.H., Pandis, S.N., 2016. Atmospheric Chemistry and Physics: from Air Pollution to Climate Change, third ed. John Wiley & Sons, Hoboken, NJ.
Shi, L., Zanobetti, A., Kloog, I., Coull, B.A., Koutrakis, P., Melly, S.J., Schwartz, J.D., 2016. Low-concentration PM2.5 and mortality: estimating acute and chronic effects in a population-based study. Environ. Health Perspect. 124, 46–52.
Simoneit, B.R.T., 2002. Biomass burning - a review of organic tracers for smoke from incomplete combustion. Appl. Geochem. 17, 129–1662.
Solomon, P.A., Crumpler, D., Flanagan, J.B., Jayanty, R.K.M., Rickman, E.E., McDade, C.E., 2014. US national PM2.5 chemical speciation monitoring networks—CSN and IMPROVE: description of networks. J. Air Waste Manag. Assoc. 64, 1410–1438.
Squizzato, S., Cazzaro, M., Innocente, E., Visin, F., Hopke, P.K., Rampazzo, G., 2017. Urban air quality in a mid-size city — PM2.5 composition, sources and identification of impact areas: from local to long range contributions. Atmos. Res. 186, 51–62.
Squizzato, S., Masiol, M., Rich, D.Q., Hopke, P.K., 2018. PM2.5 and gaseous pollutants in New York State during 2005-2016: spatial variability, temporal trends, and economic influences. Atmos. Environ. 183, 209–224.
Stafoggia, M., Cesaroni, G., Peters, A., Andersen, Z.J., Badaloni, C., Beelen, R., Caracciolo, B., Cyrys, J., de Faire, U., de Hoogh, K., Eriksen, K.T., 2014. Long-term exposure to ambient air pollution and incidence of cerebrovascular events: results from 11 European cohorts within the ESCAPE project. Environ. Health Perspect. 122, 919–925.
Straif, K., Cohen, A., Samet, J. (Eds.), 2013. Air Pollution and Cancer. IARC Scientific Publications No. 161. International Agency for Research on Cancer, Lyon Cedex, France 2013. Available at: http://www.iarc.fr/en/publications/books/sp161/AirPollutionandCancer161.pdf.
Strak, M., Janssen, N.A., Godri, K.J., Gosens, I., Mudway, I.S., Cassee, F.R., Lebret, E., Kelly, F.J., Harrison, R.M., Brunekreef, B., Steenhof, M., 2012. Respiratory health effects of airborne particulate matter: the role of particle size, composition, and oxidative potential-the RAPTES project. Environ. Health Perspect. 120, 1183–1189.
Taiwo, A.M., Harrison, R.M., Shi, Z., 2014. A review of receptor modelling of industrially emitted particulate matter. Atmos. Environ. 97, 109–120.
Thorpe, A., Harrison, R.M., 2008. Sources and properties of non-exhaust particulate matter from road traffic: a review. Sci. Total Environ. 400, 270–282.
Thurston, G.D., Burnett, R.T., Turner, M.C., Shi, Y., Krewski, D., Lall, R., Ito, K., Jerrett, M., Gapstur, S.M., Diver, W.R., Pope III, C.A., 2016. Ischemic heart disease mortality and long-term exposure to source-related components of US fine particle air pollution. Environ. Health Perspect. 124, 785–794.
Tolocka, M.P., Solomon, P.A., Mitchell, W., Norris, G.A., Gemmill, D.B., Wiener, R.W., Vanderpool, R.W., Homolya, J.B., Rice, J., 2001. East versus west in the US: chemical characteristics of PM2. 5 during the winter of 1999. Aerosol Sci. Technol. 34, 88–96.
Uria-Tellaetxe, I., Carslaw, D.C., 2014. Conditional bivariate probability function for source identification. Environ. Model. Software 59, 1–9.
USEPA, 2007. EPA superfund program: HQ_Lead targeted site identification project. Availbale at. https://www.documentcloud.org/documents/216323-epa-hq-lead-smelter-site-project-report-jan2007.html.
USEPA, 2015. Action Memorandum for an Emergency Removal Action at the Lumen Bearing Co. Site, Erie County, Buffalo, New York.
Viana, M., Pandolfi, M., Minguillón, M.C., Querol, X., Alastuey, A., Monfort, E., Celades, I., 2008. Inter-comparison of receptor models for PM source apportionment: case study in an industrial area. Atmos. Environ. 42, 3820–3832.
Watson, J.G., Zhu, T., Chow, J.C., Engelbrecht, J., Fujita, E.M., Wilson, W.E., 2002. Receptor modeling application framework for particle source apportionment. Chemosphere 49, 1093–1136.
Watson, J.G., Chow, J.C., Chen, L.W.A., Frank, N.H., 2009. Methods to assess carbonaceous aerosol sampling artifacts for IMPROVE and other long-term networks. J. Air Waste Manag. Assoc. 59, 898–911.
Weichenthal, S.A., Lavigne, E., Evans, G.J., Godri Pollitt, K.J., Burnett, R.T., 2016. PM2. 5 and emergency room visits for respiratory illness: effect modification by oxidative potential. Am. J. Respir. Crit. Care Med. 194, 577–586.
Weitkamp, E.A., Lipsky, E.M., Pancras, P.J., Ondov, J.M., Polidori, A., Turpin, B.J., Robinson, A.L., 2005. Fine particle emission profile for a large coke production facility based on highly time-resolved fence line measurements. Atmos. Environ. 39, 6719–6733.
Zhang, Q., Jimenez, J.L., Worsnop, D.R., Canagaratna, M., 2007. A case study of urban particle acidity and its influence on secondary organic aerosol. Environ. Sci. Technol. 41, 3213–3219.
Zhao, W., Hopke, P.K., 2006. Source identification for fine aerosols in mammoth cave national park. Atmos. Res. 80, 309–322.
Zhao, Y., Nguyen, N.T., Presto, A.A., Hennigan, C.J., May, A.A., Robinson, A.L., 2016. Intermediate volatility organic compound emissions from on-road gasoline vehicles and small off-road gasoline engines. Environ. Sci. Technol. 50, 4554–4563.